Rhodium self-powered neutron detector as a suitable on-line thermal neutron flux monitor in BNCT treatments

Marcelo E. Miller[a)] and Manuel L. Sztejnberg
Comisión Nacional de Energía Atómica, Av. del Libertador 8250, Ciudad de Buenos Aires 1429, Argentina

Sara J. González
Comisión Nacional de Energía Atómica, Av. del Libertador 8250, Ciudad de Buenos Aires 1429, Argentina and CONICET, Av. Rivadavia 1917, Ciudad de Buenos Aires 1033, Argentina

Silvia I. Thorp, Juan M. Longhino, and Guillermo Estryk
Comisión Nacional de Energía Atómica, Av. del Libertador 8250, Ciudad de Buenos Aires 1429, Argentina

(Received 15 April 2010; revised 1 September 2011; accepted for publication 22 October 2011; published 16 November 2011)

Purpose: A rhodium *self-powered neutron detector* (Rh SPND) has been specifically developed by the Comisión Nacional de Energía Atómica (CNEA) of Argentina to measure locally and in real time thermal neutron fluxes in patients treated with boron neutron capture therapy (BNCT). In this work, the thermal and epithermal neutron response of the Rh SPND was evaluated by studying the detector response to two different reactor spectra. In addition, during clinical trials of the BNCT Project of the CNEA, on-line neutron flux measurements using the specially designed detector were assessed.

Methods: The first calibration of the detector was done with the well-thermalized neutron spectrum of the CNEA RA-3 reactor thermal column. For this purpose, the reactor spectrum was approximated by a Maxwell–Boltzmann distribution in the thermal energy range. The second calibration was done at different positions along the central axis of a water-filled cylindrical phantom, placed in the mixed thermal–epithermal neutron beam of CNEA RA-6 reactor. In this latter case, the RA-6 neutron spectrum had been well characterized by both calculation and measurement, and it presented some marked differences with the ideal spectrum considered for SPND calibrations at RA-3. In addition, the RA-6 neutron spectrum varied with depth in the water phantom and thus the percentage of the epithermal contribution to the total neutron flux changed at each measurement location. Local (one point-position) and global (several points-positions) and thermal and mixed-field thermal neutron sensitivities were determined from these measurements. Thermal neutron flux was also measured during BNCT clinical trials within the irradiation fields incident on the patients. In order to achieve this, the detector was placed on patient's skin at dosimetric reference points for each one of the fields. System stability was adequate for this kind of measurement.

Results: Local mixed-field thermal neutron sensitivities and global thermal and mixed-field thermal neutron sensitivities derived from measurements performed at the RA-6 were compared and no significant differences were found. Global RA-6-based thermal neutron sensitivity showed agreement with pure thermal neutron sensitivity measurements performed in the RA-3 spectrum. Additionally, the detector response proved nearly unchanged by differences in neutron spectra from real (RA-6 BNCT beam) and ideal (considered for calibration calculations at RA-3) neutron source descriptions. The results confirm that the special design of the Rh SPND can be considered as having a pure thermal response for neutron spectra with epithermal-to-thermal flux ratios up to 12%. In addition, the linear response of the detector to thermal flux allows the use of a mixed-field thermal neutron sensitivity of $1.95 \pm 0.05 \times 10^{-21}$ A $n^{-1}\cdot cm^2\cdot s$. This sensitivity can be used in spectra with up to 21% epithermal-to-thermal flux ratio without significant error due to epithermal neutron and gamma induced effects. The values of the measured fluxes in clinical applications had discrepancies with calculated results that were in the range of −25% to +30%, which shows the importance of a local on-line independent measurement as part of a treatment planning quality control system.

Conclusions: The usefulness of the CNEA Rh SPND for the on-line local measurement of thermal neutron flux on BNCT patients has been demonstrated based on an appropriate neutron spectra calibration and clinical applications. [DOI: 10.1118/1.3660204]

Key words: SPND, BNCT, on-line flux measurement

I. INTRODUCTION

Boron neutron capture therapy (BNCT) consists of the action of heavy ions produced by neutron capture in ^{10}B nuclei that have been selectively localized in tumor cells via a suitable boron-labeled delivery agent. The ^{10}B neutron capture cross section is 3838 barns at 2200 m/s (Ref. 1) and decreases rapidly for higher neutron energies. (Throughout this work, neutron spectra will be classified according to neutron energies as follows: thermal neutrons, for energies up to 0.4 eV, epithermal neutrons, for energies ranging from 0.4 eV to 10 keV, and fast neutrons, for energies greater than 10 keV.) The thermal neutron flux and boron biodistribution in the irradiation volume are very important factors concerning the dose delivered to patients in BNCT. Thus their accurate assessment during the irradiation is essential for the quality assurance of the treatment.

In a typical clinical trial, a treatment plan is developed before irradiation to determine the optimum attainable irradiation conditions. A complex computational system, called *treatment planning system* (TPS), is used for that purpose. TPS takes into account patient anatomy, patient positioning, characteristics of the nuclear reactor beam supplying the neutrons, and ^{10}B concentrations. TPS offers an estimation of the dose distribution in the patient as a result. This dose distribution consists of a mixture of different components that result from neutron capture, neutron scattering, and incident gamma rays that are present to some extent in any practical neutron beam.

Before and during the treatment procedure, attempts are made to meet plan conditions primarily through three actions: testing of blood boron concentration, reproduction of geometry, and monitoring of the beam. The former takes place after infusion of the boron compound and continues until blood ^{10}B concentration is acceptable to begin irradiation. Usually, blood sampling also takes place after irradiation for retrospective analysis. The second action is ordinarily completed during patient positioning just before irradiation with the aid of laser positioning devices and other tools. Once the irradiation begins, positioning can only be followed by a video camera. In order to more efficiently perform the positioning for the actual irradiation, a simulation is usually carried out at planning time in a simulation room. The third action is generally accomplished through the use of beam monitors (e.g., fission chambers) located as closely as possible to the irradiation port. Their goal is to obtain on-line measurements of the neutron source in order to confirm or correct assumed planning conditions. If measured fluxes are different from fluxes assumed for planning, corrections can be made, e.g., in reactor power and/or in treatment irradiation time. However, fluxes obtained from beam monitors are still not fluxes in the actual patient treatment volume delineated in the treatment planning process. Therefore, the fact that fluxes at the beam monitor location may be equal to those from planning does not imply the same for fluxes within the patient.

I.A. Local flux real-time detection

The primary accepted method for the detailed, high-resolution determination of local neutron fluxes is based on the so-called activation technique. However, since this method does not produce real-time results for the measurement of the neutron flux, it is primarily used for retrospective analyses. On the other hand, silicon diodes, planar silicon p-i-n diodes, and MOSFETs can be found among real-time methods for flux measurement in BNCT.[2–6] For in-patient measurements, a real-time thermal neutron flux monitor based on boron or lithium-loaded plastic scintillator coupled to an optical fiber for locally monitoring fluxes during BNCT irradiations was used in Japan.[7,8]

In the present work, a novel method for local flux real-time detection is presented that was specifically developed for NCT applications. It is based on the use of a *self-powered neutron detector* (SPND) with a particular design that can be placed over the skin or, alternatively, can be implanted under the skin of patients due to its small external dimensions.[9,10] As compared to detectors based on plastic scintillators, an SPND-based measurement system is not ordinarily subject to signal saturation problems for high neutron capture rates, using rhodium as the sensitive SPND material features a lower burn-up rate than boron- or lithium-based systems and rhodium SPNDs offer a gamma sensitivity low enough to allow neglecting the incident gamma contribution present in typical BNCT irradiation fields. The detector of interest here is a cylindrical 3-part assembly that includes a cylindrical inner emitter made of ^{103}Rh, an acrylic insulator tube, and an outer collector sheath made of Zircaloy-4. This SPND also has a BNC-connector-ended low-noise coaxial cable as transmission media that connects it to the measurement electronics. The cable type is low-triboelectric-noise RG 174/U, which is commonly used for nuclear instrumentation.[16] The special design of the cable reduces significantly the triboelectric effect (spurious currents due to cable movements). Compared with optical fiber, this cable presents a much greater flexibility that allows an easier handling and detector positioning. However, another factor to consider is that radiation delivered to a part of the cable can also induce a current. The potential magnitude of this current must be evaluated in order to assure this does not interfere unacceptably with the actual measurement.

In this type of devices, the ^{103}Rh central emitter captures neutrons, yielding ^{104}Rh with subsequent beta decay via two channels having half lives of 43 s (92.4%) and 4.4 min (7.8%). The emitted beta particles have enough energy to reach the external sheath after passing through the acrylic isolation, thus creating a potential difference across the device. If an electrometer is connected between central rhodium electrode and the external sheath, this potential difference produces a continuous current that is proportional to the neutron flux. These detectors also have a gamma response due to photoelectric and Compton effects that can also produce free electrons with enough energy to pass from the emitter to the external sheath or vice versa. Both types of interaction can also be present in the detector cable but, in that case, the response to neutron and gamma radiation is much lower than the detector response to neutrons.

The probability per unit time of ^{103}Rh capturing a neutron with energy between E and $E+dE$ is proportional to the

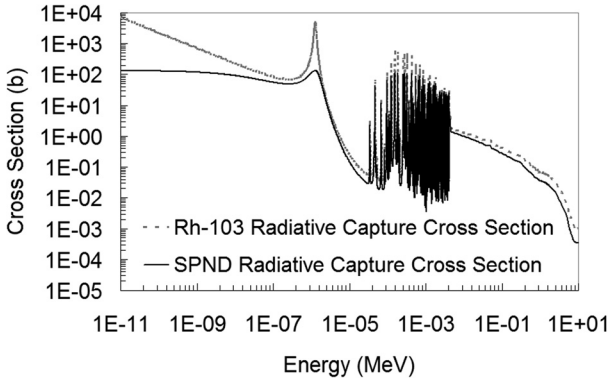

FIG. 1. ^{103}Rh and SPND radiative capture cross section as a function of energy (Ref. 11).

product $\Phi(E)\ \sigma(E)$, where $\Phi(E)$ and $\sigma(E)$ are the energy-dependent neutron flux and capture cross section, respectively. As can be determined from Fig. 1, ^{103}Rh has a thermal neutron capture cross section of 147 barns at 0.0253 eV, with a general decreasing behavior with neutron energy, but with an important resonance peak in the epithermal energy range around 1 eV.[11] It is important to note that below 0.4 eV ^{103}Rh thermal neutron capture cross section is of the type $1/v$ as well as the one for ^{10}B. FIG. 1 also illustrates the SPND radiative capture cross section that was estimated specifically for the detector presented in this work by means of MCNP (Ref. 12) neutron transport simulations. This is the effective capture cross section in the detector body, which includes the rhodium self-shielding effect. Corresponding to this effect, the figure shows a large reduction of the highest values of the cross section, which implies a reduction of the importance of the resonances in the detector response. Due to the patterns of these cross sections, rhodium Rh SPNDs show a very good response to thermal neutrons but they still also present some response to epithermal neutrons that has not been evaluated yet for our particular design. One of the objectives of this work is to characterize the thermal and epithermal response of the Rh SPND in order to evaluate its suitability as an instrument to perform thermal flux measurements in real NCT beams, and particularly, in the clinical trials that employ the RA-6 reactor NCT beam.

I.B. Measurements in clinical trials

The SPND based novel detection method was developed by the Comisión Nacional de Energía Atómica of Argentina (CNEA) in the frame of the argentine BNCT Project. In 2003, the Administración Nacional de Medicamentos, Alimentos y Tecnología (ANMAT), and the Autoridad Regulatoria Nuclear (ARN) approved the BNCT Project Phase I/II clinical trial (ANMAT 3976-2003 and ARN 21190-2003, respectively). The protocol was designed to evaluate the efficacy and toxicity of BNCT for skin melanomas in extremities. It involves single administrations of BPA-fructose boron compound followed by single fraction neutron beam irradiations. These irradiations are performed at the BNCT facility available at the RA-6 reactor located at the Centro Atómico Bariloche (CAB), CNEA.[13]

As part of Phase I/II melanoma BNCT clinical trial conducted in Argentina seven patients to date have received eight treatment sessions covering ten anatomical areas located in extremities. All patients presented multiple subcutaneous skin metastases of melanoma on their right or left leg.[14,15]

The performance of the novel detection method presented in this article under actual BNCT irradiation conditions was evaluated during the treatments of patients 3, 4, 5, and 6. The purpose of this evaluation was to demonstrate the feasibility of *in situ* monitoring of the irradiation field, with special emphasis on evaluating the stability and accuracy of the measurement system.

The treated patients had nodular melanoma progression in different regions of their legs.[14] Patients' nodules in the target area were labeled and delineated on the CT scans performed prior to the irradiation for evaluation purposes. The detector was positioned according to treatment planning and the measurement results were compared to the estimated values from the treatment planning calculations.

II. MATERIALS AND METHODS

II.A. Measurement system

The measurement system used for evaluating thermal and epithermal response of the SPND design of interest and for measurements during the clinical trials was composed of the Rh SPND itself (serial number CNEA Rh-10), low current electrometers, and a PC.

The particular design of the SPND used in this work had an emitter of 10 mm length and 1 mm diameter, a design that balances different detector characteristics such as sensitivity, size, flux depression, and electron self-shielding. The overall detector size was 1.9 mm diameter and 15 mm length.

According to the simplest response form of an SPND,[9,16] the expected CNEA Rh-10 sensitivity would be expected to range from 10^{-21} to 10^{-20} A·n^{-1}·cm^2·s. Typical BNCT thermal neutron fluxes range from 10^8 to 10^{10} n·cm^{-2}·s^{-1}. Consequently, currents for this type of detection range from 10^{-13} to 10^{-10} A. Therefore, Keithley electrometers, models 6517A and 6514, both with a resolution of 0.1 fA were used to obtain high quality readings. Readings from the electrometers were always displayed and recorded in real time in a PC.

The stability of the entire SPND measurement system was characterized by a reading standard deviation of 1 fA for a series of measurements over a time period of more than 10 h under no radiation fields.

The measurement of SPND current began some minutes before the start of irradiation and ended some minutes after the end. The recorded currents during irradiation, i_r, were used to obtain a time-average current, I_r. Readings before and after each irradiation field, i_0, were time-averaged to determine the system *offset current*, I_0 (current without irradiation). The average current generated by the applied radiation field, I_m, is calculated as $I_m = I_r - I_0$.

II.B. Part A: Detector sensitivity characterization

II.B.1. Definitions

The measured current (I_m) of the rhodium-based SPND irradiated in a mixed neutron and gamma radiation field can be expressed as

$$I_m = I_{th} + I_{epi} + I_{\gamma_{(d+c)}}, \tag{1}$$

where each term represents the contributions to the total current due to the interaction of the detector with the thermal neutron flux (I_{th}), the epithermal neutron flux (I_{epi}), and the interaction of the detector and cable with gamma flux ($I_{\gamma_{(d+c)}}$). Since the rhodium capture cross section is low and rapidly decreasing for neutron energies greater than 10 keV (Fig. 1), the interaction of the detector with fast neutrons can be considered negligible in a thermal irradiation.

The detector sensitivity for thermal (S_{th}) and epithermal (S_{epi}) contributions can be defined as

$$S_i = \frac{I_i}{\Phi_i}, \tag{2}$$

where Φ denotes neutron flux (in $\text{n}\cdot\text{cm}^{-2}\cdot\text{s}^{-1}$) for component i. Combining Eqs. (1) and (2), the thermal neutron sensitivity can be expressed as

$$S_{th} = \frac{I_m - I_{epi} - I_{\gamma_{(d+c)}}}{\Phi_{th}}. \tag{3}$$

According to this equation, the determination of the SPND thermal neutron sensitivity requires quantification of not only the partial and total currents but also the thermal neutron flux at the calibration position.

The detector and cable gamma sensitivity per irradiated centimeter is defined as

$$S_{\gamma_{(d+c)}} = \left(\frac{I_{\gamma_{(d+c)}}}{l_{\gamma_{(d+c)}}\dot{D}_\gamma}\right), \tag{4}$$

where $\dot{D}_\gamma$ is the gamma dose rate (in $\text{mGy}\cdot\text{h}^{-1}$) and $l_{\gamma_{(d+c)}}$ is the length of detector and cable (in cm) under a non-negligible gamma field. This sensitivity was determined by irradiating the detector and a well known cable length in a pure gamma field, using ^{60}Co and ^{137}Cs gamma sources.

II.B.2. SPND calibration

It is clear from previous considerations that the relative contributions of I_{th} and I_{epi} to the measured total current depend on the neutron spectrum characteristics. In order to evaluate S_{th} and S_{epi} of the SPND under different spectra, two detector calibrations were performed. The first one was done inside the thermal column of the RA-3 reactor[17] and the second one was carried out at different positions along the central axis of a water-filled cylindrical phantom, placed with one end adjacent to the irradiation port of the original RA-6 BNCT beam.[13] Different irradiation configurations were used in both facilities. Within the RA-3 thermal column, the SPND is surrounded by a nearly uniform neutron field, and more than a meter of cable is exposed to considerable radiation levels. In RA-6 BNCT facility, a beam-like irradiation with just a few centimeters of exposed cable was the available setup.

II.B.2.a. Calibration at RA-3 thermal column. In order to evaluate spectrum characteristics close to the calibration positions, bare and cadmium-covered gold activation foils were irradiated inside the thermal column. The cadmium ratio obtained from these measurements was 4100,[18] which demonstrates that selected calibration positions present a well-thermalized neutron spectrum. Assuming thus that the epithermal contribution to the total current can be considered negligible for these calibration positions, Eq. (3) can be simplified to

$$S_{th} = \frac{I_m - I_{\gamma_{(d+c)}}}{\Phi_{th}}. \tag{5}$$

A detailed measured gamma profile along the small tube where detectors and cables pass through to the irradiation position was not practically obtainable. Therefore, a second detector with very similar geometry and materials to those for CNEA Rh-10 but with an emitter made of Zry-4 (Zircaloy-4, a Zr based alloy) was used to evaluate $I_{\gamma_{(d+c)}}$.[9] Since Zry-4 neutron capture cross section is very low, the response of this detector to neutrons can be considered negligible. Thus, the measured total current with Zry-4 detector is basically due to the interaction of the detector and irradiated cable with the gamma flux (i.e., $I_m^{\text{Zy}-4} \approx I_{\gamma_{(d+c)}}^{\text{Zy}-4}$). Additionally, since zirconium and rhodium atomic numbers are similar ($Z = 40$ and $Z = 45$, respectively), the gamma sensitivity of both detectors can be considered approximately equal, $I_m^{\text{Zy}-4} \approx I_{\gamma_{(d+c)}}$. An estimation of the current $I_{\gamma_{(d+c)}}$ is thus obtained by placing the Zry-4 detector and cable parallel to the Rh SPND. Considering this estimation, Eq. (5) can be rewritten as

$$S_{th} = \frac{I_m - I_m^{\text{Zy}-4}}{\Phi_{th}}. \tag{6}$$

The calibration procedure involved several measurements in the graphite thermal column with a reactor power of 5 MW. In each column location, both Rh and Zry-4 detectors were installed with their active zones at the same distance from the reactor core. Currents were measured simultaneously with two Keithley electrometers (models 6514 and 6517A) connected to a PC. Mean measured currents and their dispersions were obtained from these data.

In order to estimate the thermal flux during irradiation, neutron activation foils and wires were simultaneously irradiated at the same distance from the reactor core as the detectors but separated laterally from them by a distance of 2 cm. Two types of activation foils were employed, namely bare Cobalt (^{59}Co), 3 mm in diameter and 0.125 mm thick, and bare Gold (^{197}Au), 3 mm in diameter and 0.02 mm thick. Activation wires used for flux measurements were approximately 10 mm in length and 1 mm in diameter and were composed of Copper alloyed with 1.55% Gold by weight. Gammas from the activated foils and wires were measured using a high-purity germanium detector (HPGe) previously calibrated using a commercial Europium (^{152}Eu) source of certified activity. (Certificate of calibration No. 76044A-440,

Eckert & Ziegler Analytics, Inc., October 30, 2007. Analytics maintain traceability to National Institute of Standards and Technology.) The Westcott formalism was used to obtain thermal flux values from the measured activities.[19] For this, the neutron spectrum at the irradiation location was assumed to have a pure Maxwell–Boltzmann distribution, thermalized to the actual material temperature (38 °C by direct measurements).

Sensitivities for each material were determined and the average of the three values was eventually taken as the final calibration factor for the SPND.

A second detector, of the same type described above, was characterized by irradiation in the RA-3 thermal column using the first detector as a reference.

II.B.2.b. Calibration at RA-6 BNCT facility. The RA-6 neutron spectrum in air has been well characterized prior to the SPND calibration irradiations described here. (The characterization of the SPND was performed before the upgrade of the RA-6 reactor in 2008.) The thermal region of the spectrum differed from the ideal Maxwell–Boltzmann spectrum assumed for RA-3 thermal column.[13] In addition, the RA-6 beam contains a mixture of thermal and epithermal neutrons. Historical measurements using bare and cadmium-covered gold foils yielded epithermal-to-thermal neutron flux ratios at the detector calibration locations of up to 25%. Thus, the epithermal contribution to the detector response is not *a priori* negligible for this beam.

According to these considerations, the methodology followed to obtain thermal neutron sensitivity and an estimation of the epithermal neutron sensitivity was different from that used in RA-3. In this case, Rh SPND measurements were performed in six different positions inside a dry acrylic tube of 10 mm internal diameter, along the central axis of a water-filled cylindrical acrylic phantom aligned axially with the neutron beam. The detector position was coaxial to the phantom and the beam and the center of the SPND sensitive zone was located at distances of 9, 12, 22, 32, 52, and 82 mm from the upstream surface of the phantom. The acrylic phantom, 17.3 cm in diameter and 20.5 cm long, was placed with its axis coincident to the central axis of the RA-6 neutron beam and adjacent to the 15 cm diameter irradiation port. The total current was acquired for each irradiation position (n) and, from these, time-averaged measured currents and their dispersions were obtained.

Substituting Eq. (2) into Eq. (1), the measured total current at each detector axial location inside the phantom (I_m^n) can be expressed as

$$I_m^n = S_{th}\Phi_{th}^n + S_{epi}\Phi_{epi}^n + I_{\gamma_{(d+c)}}^n. \tag{7}$$

In contrast to the RA-3-based calibration procedure, $I_{\gamma_{(d+c)}}^n$ in Eq. (6) were calculated rather than measured directly. In order to perform these calculations, the total cable length inside the phantom (the cable outside the phantom was considered to be in a negligible gamma field), the previously obtained gamma sensitivity per irradiated centimeter of both detector and cable, and the total gamma dose rate profile along the phantom were considered. Gamma (and fast neutron) dose profiles were measured using the paired ionization chamber (IC) method. Selected ICs were miniature Far West Tech. model IC-18 (A-150 TE plastic, 0.1 cm^3 gas cavity, flushed with methane-based TE gas) and model IC-18G (graphite, 0.1 cm^3 gas cavity, flushed with high purity carbon dioxide). The IC-18G was used as the detector with low neutron sensitivity.

A set of bare activation wires of copper alloyed with 1.55% gold by weight (1 mm diameter and approximately 10 mm length) was irradiated without the Rh SPND present to obtain thermal and epithermal flux profiles along the central axis of the phantom. The neutron absorption in ^{63}Cu and ^{197}Au provides two activation responses that were used to determine, through the two-material method, the thermal and epithermal neutron flux contribution at each wire location. For each wire and irradiation position, the gamma self-absorption and neutron self-shielding factors together with an average thermal neutron capture cross section were evaluated through MCNP calculations. Finally, at each detector calibration position, thermal and epithermal fluxes in Eq. (7) were obtained by interpolation.

All measured total currents and estimated thermal and epithermal fluxes during this calibration were normalized to a fixed BNCT irradiation port beam monitor value of 320 mV.

An over-determined system of six linear equations, Eq. (7), with two unknowns (S_{th} and S_{epi}) was obtained by combining all the data and solved by standard least-squares fitting methods. These sensitivities will be referred as global.

Additionally, for each irradiation position n, a raw thermal neutron sensitivity, named local mixed-field thermal neutron sensitivity, was obtained as

$$S_{mix}^n = \frac{I_m^n}{\Phi_{th}^n}. \tag{8}$$

The *global mixed-field* thermal neutron sensitivity, S_{mix}, was obtained by fitting $\Phi_{th}^n S_{mix} = I_m^n$ to the six measurement points (six equations with one unknown, S_{mix}) using standard least-squares fitting methods. This sensitivity is intended to be used for the thermal flux measurement during the BNCT treatments since it simplifies the process through the single measurement of the total current. The range of validity of the calculated S_{mix} is given by the epithermal-to-thermal neutron flux ratio range from the measurements.

II.C. Part B: Clinical trial measurements

II.C.1. Treatment planning and detector position selection

The locations of the SPND were selected to be consistent with reference positions, or marker points, set for treatment planning. They were selected in an effort to obtain fluxes as high as possible in accessible positions over the patient. Thermal neutron flux assessment was the main goal of the task. The estimation of the values of the radiation fields in these points was calculated by means of a TPS, in this case, NCTPlan.[20,21]

NCTPlan creates a voxelized patient anatomical model as input for MCNP (Ref. 12) calculations specific to the

position of the patient relative to the reactor irradiation port (with a 15 cm diameter beam aperture), the beam characteristics, the tissues involved in the irradiation volume, and the ^{10}B concentration. In typical BNCT planning, the results show the expected dose distribution within the patient. However, for this case, additional output was required and few changes in the process were made in order to obtain neutron fluxes as result. When these values were calculated, the points for SPND localization could be chosen.

Several patients were irradiated at RA-6 with the SPND placed according to guidance from the treatment plan results specific to each patient as noted above. Patient 3 (L.G.) was exposed to a 3-site irradiation, one field each site. One of the fields was in her calf (C1), another slightly above her heel (C2), and the other in her foot sole (C3). All of them were in the right leg. Patients 4, 5, and 6 (named M.T.M., M.C.G., and A.E.S., respectively) were exposed to single field irradiation in their leg, heel, and thigh, respectively.[14,15] It should be noted that only a few centimeters of detector-cable were under considerable gamma exposition during the treatment. This was achieved by careful alignment of the detector and cable to minimize the amount of exposed cable. Figure 2 shows an example of the positioning of the detector during treatment simulations and irradiations.

Considering SPND positioning, some dependence of the detector sensitivity on the angle between detector axis and beam direction might be expected. In order to evaluate the difference between the experimentally determined sensitivity and the sensitivity associated to the actual detector position in each treated patient, MCNP5-based simulations were performed. When the above mentioned angle lies between 45° and 90°, the difference is at most of 10%. It should be noted that this range of angles includes the most likely cases regarding the actual possibility of locating the sensor over the patients, as it happens in the presented clinical cases (Fig. 2).

The CNEA Rh-10 signal, a signal from the beam monitor, and the patient positioning were recorded during each irradiation. In the case that the latter two parameters are stable, the former should also be stable under normal operating conditions.

II.C.2. Comparison parameters

In order to make a comparison between expected values from the treatment planning and measured values, the following quantities were evaluated:

$$\Phi_{th}^{m} = \frac{I_m}{S_{mix}}, \tag{9}$$

$$\Delta^{\%}\Phi_{th} = 100\,\frac{\Phi_{th}^{m} - \Phi_{th}^{c}}{\Phi_{th}^{c}}, \tag{10}$$

where Φ_{th}^{m} and Φ_{th}^{c} are the measured and calculated thermal neutron fluxes, and $\Delta^{\%}\Phi_{\mathrm{th}}$ is the percent relative difference between measured and estimated fluxes. Because the CNEA Rh-10 SPND exhibits the usual time delay in its response, signal steady state was assumed to have occurred 15 min after any change in reactor power.

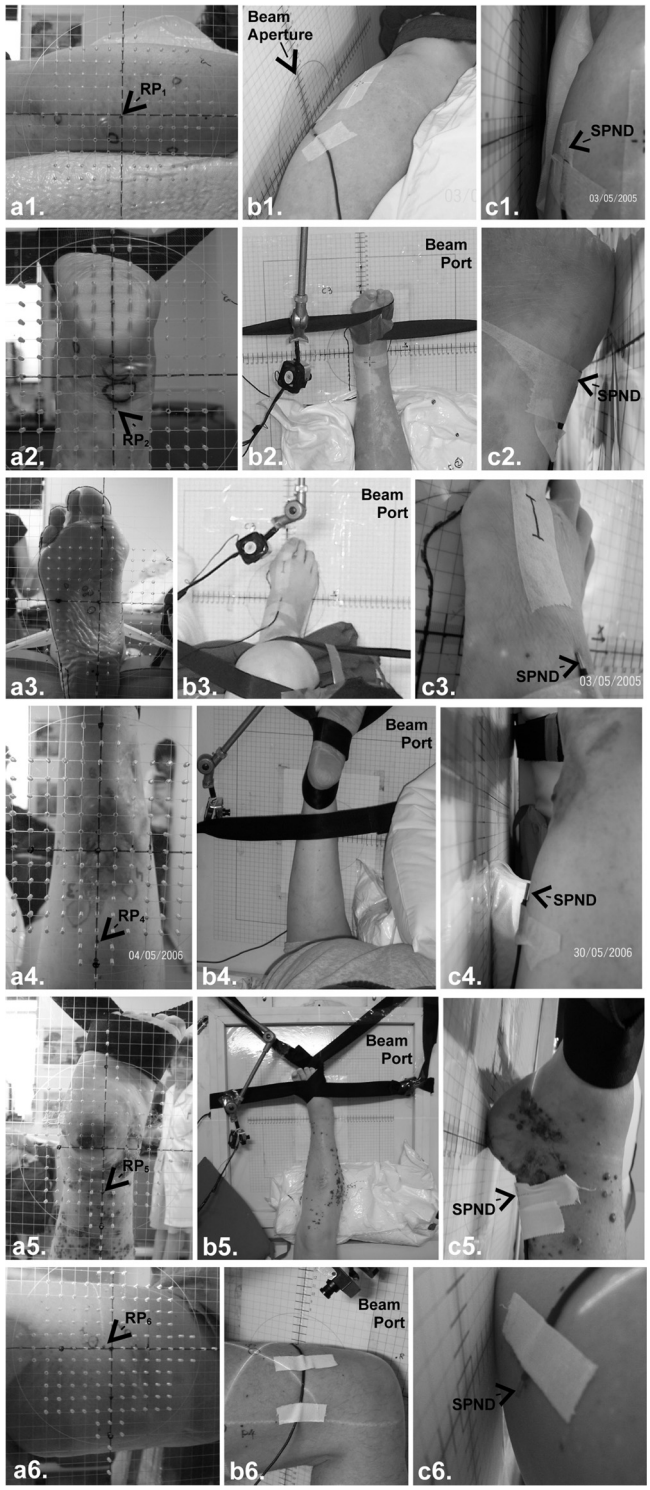

FIG. 2. Photograph of the detector positioning for irradiations: (1) patient 3, C1; (2) patient 3, C2; (3) patient 3, C3; (4) patient 4; (5) patient 5; and (6) patient 6. (a) Beam's eye view in the simulation room (the surface with grid-lines is that of the irradiation port; RP: reference point for locating the SPND); (b) irradiation set-up at RA-6 reactor; (c) SPND location on the patient skin during irradiation.

III. RESULTS

III.A. Part A: Detector sensitivity characterization

This section presents the results of the Rh SPND neutronic and gamma calibration experiments.

TABLE I. Results of the Rh SPND calibration experiment at the RA-3 thermal column: measured total currents with rhodium (I_m) and Zry-4 detectors ($I_m^{\mathrm{Zry-4}}$), estimated thermal neutron fluxes (Φ_{th}) and thermal neutron sensitivity (S_{th}) for each activation material, and the resulting Rh SPND thermal neutron sensitivity ($S_{th}^{\mathrm{averaged}}$).

Irradiation	I_m (pA)	$I_m^{\mathrm{Zry-4}}$ (pA)	Activation material	Φ_{th} (10^9 n·cm^{-2}·s^{-1})	S_{th} (10^{-21} A·n^{-1}·cm^2·s)	$S_{th}^{\mathrm{averaged}}$ (10^{-21} A·n^{-1}·cm^2·s)
1	13.30 ± 0.13	1.11 ± 0.03	Co foil	6.6 ± 0.2	1.85 ± 0.06	1.90 ± 0.08
2	12.1 ± 0.3	0.70 ± 0.03	Co foil	5.87 ± 0.07	1.94 ± 0.06	
1	13.30 ± 0.13	1.11 ± 0.03	Cu/Au wire	6.8 ± 0.3	1.79 ± 0.08	1.79 ± 0.09
3	11.75 ± 0.06	0.66 ± 0.01	Cu/Au wire	6.2 ± 0.1	1.79 ± 0.03	
1	13.30 ± 0.13	1.11 ± 0.03	Au foil	6.8 ± 0.2	1.79 ± 0.06	1.79 ± 0.06
Mean thermal neutron sensitivity						1.83 ± 0.10

The obtained gamma sensitivity per irradiated centimeter of both detector and cable, $S_{\gamma(d+c)}$, was $2.2 \pm 0.5 \times 10^{-15}$ A·mGy^{-1}·h·cm^{-1}.

Concerning neutron response, Table I shows the steady state measured total currents with rhodium and Zry-4 detectors for each irradiation at RA-3, the estimated thermal neutron fluxes for each activation material, and the resulting Rh SPND thermal neutron sensitivity. Statistical uncertainties in I_m and $I_m^{\mathrm{Zry-4}}$ correspond to one standard deviation of the current values during the irradiation time, after saturation was reached, and include reactor power variations. Using the values from Table I, a mixed-field thermal neutron sensitivity was calculated (without subtracting gamma induced currents), yielding a value of $1.97 \pm 0.06 \times 10^{-21}$ A·n^{-1}·cm^2·s.

Table II lists Rh SPND measured total currents, estimated currents due to gamma field, and corresponding thermal and epithermal neutron flux values for each SPND axial location inside the cylindrical phantom irradiated in the RA-6 beam. The solution of the system of Eqs. (7), which determines the global thermal and epithermal neutron sensitivities, as well as the global mixed-field thermal neutron sensitivity are summarized in the same table. Table II also shows the local mixed-field thermal neutron sensitivities for each irradiation position. Recall that these sensitivities are obtained using the total measured current of the Rh SPND without subtracting gamma and epithermal contributions.

Figure 3 shows the response of the detector in terms of the measured current as a function of the thermal flux. This response was obtained from the *in-phantom* measurements at the RA-6 BNCT facility, where increasing thermal fluxes represent decreasing thermal-to-total flux ratios (also in Fig. 3).

The second detector calibrated using the first one as reference was found to be approximately 4% less sensitive, exhibiting a value of S_{mix} equal to $1.88 \pm 0.05 \times 10^{-21}$ A·n^{-1}·cm^2·s.

III.B. Part B: Clinical trial measurements

The values of thermal and epithermal neutron flux (Φ_{th}) were obtained for reference points associated with the geometries of the different treatments using NCTPlan and SPHERE.[15,22,23] These fluxes and the expected theoretical ($I_c = S_{\mathrm{mix}}\Phi_{\mathrm{th}}$) and measured currents (I_m) are detailed in Table III. Quoted uncertainties for these values include a conservative estimate of the uncertainty due to the voxelization performed by the dosimetry system (NCTPlan and SPHERE). For this case, S_{mix} was $1.88 \pm 0.05 \times 10^{-21}$ A·n^{-1}·cm^2·s since the second detector was used for these measurements. This table also shows the percentage difference ($\Delta^{\%}\Phi_{\mathrm{th}}$) between the calculated fluxes from the planning and the SPND based measurements.

Figure 4 shows the readings of the Rh SPND, i_r, and the estimated currents, I_c, for the irradiations of patients 3 to 6. The beam monitor during the irradiations of patient 3 is also presented in the figure.

IV. DISCUSSION

IV.A. Rh SPND characterization

The results reported in Table II show that the value of $1.95 \pm 0.05 \times 10^{-21}$ A·n^{-1}·cm^2·s obtained for the mixed-field thermal neutron sensitivity appropriately matches the local mixed-field thermal neutron sensitivities and is

TABLE II. Results of the Rh SPND phantom measurements at the RA-6 BNCT facility: experimental currents (I_m and $I_{\gamma(d+c)}$) and fluxes (Φ_{th} and Φ_{epi}), local mixed-field thermal neutron sensitivity (S_{mix}^n); and global thermal (S_{th}), epithermal (S_{epi}), and mixed-field thermal neutron sensitivities (S_{mix}). (Goodness of fit: $R^2 = 0.9998$ and $RMSE = 9$ fA for S_{th} and S_{epi}, and $R^2 = 0.9997$ and $RMSE = 13$ fA for S_{mix}.)

Depth (MM)	I_m (pA)	$I_{\gamma(d+c)}$ (PA)	Φ_{th} (10^8 n·cm^{-2}·s^{-1})	Φ_{epi} (10^8 n·cm^{-2}·s^{-1})	Φ_{epi}/Φ_{th} (%)	S_{mix}^n (10^{-21} A·n^{-1}·cm^2·s)
9	1.925 ± 0.005	0.020 ± 0.003	9.82 ± 0.34	2.07 ± 0.25	21 ± 3	1.96 ± 0.07
12	1.853 ± 0.005	0.019 ± 0.003	9.47 ± 0.54	1.72 ± 0.26	18 ± 3	1.96 ± 0.11
22	1.484 ± 0.004	0.016 ± 0.002	7.55 ± 0.42	0.978 ± 0.132	13 ± 1	1.97 ± 0.11
32	1.112 ± 0.003	0.014 ± 0.002	5.82 ± 0.33	0.445 ± 0.073	8 ± 1	1.91 ± 0.11
52	0.578 ± 0.003	0.010 ± 0.002	2.99 ± 0.37	0.122 ± 0.024	4 ± 1	1.93 ± 0.24
82	0.194 ± 0.003	0.006 ± 0.001	1.00 ± 0.14	0.0371 ± 0.0066	4 ± 1	1.94 ± 0.27
Sensitivity (10^{-21} A·n^{-1}·cm^2·s)			$S_{\mathrm{th}} = 1.89 \pm 0.13$	$S_{\mathrm{epi}} = 0.3 \pm 0.8$		$S_{\mathrm{mix}} = 1.95 \pm 0.05$

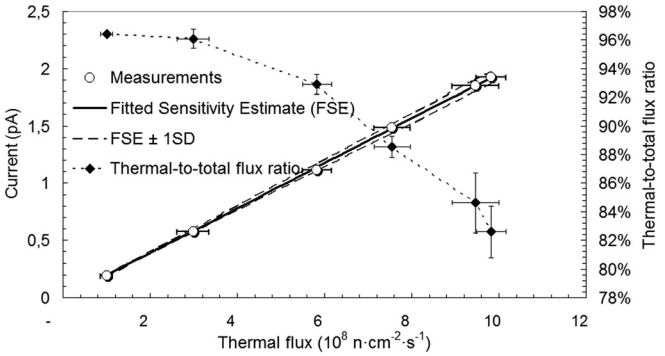

FIG. 3. Rh SPND response to *in-phantom* irradiations at RA-6 BNCT facility. The thermal-to-total flux ratio is also presented.

statistically similar to the pure thermal neutron sensitivities of $1.83 \pm 0.10 \times 10^{-21}$ A·n^{-1}·cm^2·s (Table I) and $1.89 \pm 0.13 \times 10^{-21}$ A·n^{-1}·cm^2·s obtained from irradiations at RA-3 and RA-6, respectively. The global thermal RA-6 based sensitivity is also in agreement with the pure thermal neutron sensitivity obtained with the RA-3 spectrum. This is an important result because it demonstrates that the thermal neutron sensitivity obtained in a highly thermalized spectrum (described by an ideal Maxwell–Boltzmann distribution and with a negligible epithermal component) can be used in mixed-spectrum BNCT neutron beams such as the one at RA-6 (i.e., spectra not strictly Maxwell–Boltzmann distributed in the thermal zone and epithermal-to-thermal ratio up to 21%).

The epithermal neutron sensitivity appears in Table II with a value of $0.3 \pm 0.8 \times 10^{-21}$ A·n^{-1}·cm^2·s, with an uncertainty larger than the absolute value. The potential negative values do not have a physical meaning and are statistical artifacts. On the other hand, the positive range reaches values that are not negligible compared to the pure thermal and mixed-field thermal neutron sensitivities. However, the epithermal neutron sensitivity is still lower than the thermal neutron sensitivity despite the high epithermal resonance peaks that occur in Rh. S_{epi} is about 16% of S_{th}, and even if the quoted uncertainty is added to S_{epi}, the sum is still only about 60% of S_{th}. When Φ_{epi}/Φ_{th} is less than 12% (less than 22 mm depth in the utilized experimental arrangement), the range of epithermal flux induced currents falls inside the one standard error band (7%) of the thermal neutron flux induced current and, consequently, the epithermal neutron effect is of limited significance (Table II). The relatively low epithermal response can be explained in terms of the self-shielding that produces flux depression in the resonance energy range and, consequently, a reduced effective detector cross section (Fig. 1). In addition to the flattening of the cross section, the shape of the beam spectrum is another important factor. The thermal neutrons are basically distributed in a 0.4 eV range where rhodium has high cross sections while the epithermal neutrons are spread over a range of 10 keV where the rhodium cross section alternates between a relatively low background capture cross section and some resonance peaks.

In terms of the practical use of the CNEA Rh-10 SPND, it is important to be able to assess the thermal flux without *a priori* detailed knowledge of the gamma and epithermal neutron fields. Accordingly, the mixed-field thermal neutron sensitivity would be the appropriate value to be used for the detector sensitivity since it includes the gamma and epithermal neutron influence within the spectral range for which it has been calibrated.

Figure 3 shows, for irradiation at RA-6 facility, the linearity between I_m and the thermal flux despite the changes of spectral composition over the calibration range and the gamma contamination that is known to be present. This can be explained by rearranging Eqs. (7) and (8) to obtain

$$S_{mix} = S_{th} + S_{epi}\frac{\Phi_{epi}}{\Phi_{th}} + \frac{I_{\gamma_{(d+c)}}}{\Phi_{th}}, \tag{11}$$

with

$$\Phi_{epi}/\Phi_{th} = \overline{\Phi_{epi}/\Phi_{th}} \pm \Delta\left(\Phi_{epi}/\Phi_{th}\right) \tag{12}$$

and

$$I_{\gamma_{(d+c)}}\Big/\Phi_{th} = \overline{I_{\gamma_{(d+c)}}\Big/\Phi_{th}} \pm \Delta\left(I_{\gamma_{(d+c)}}\Big/\Phi_{th}\right), \tag{13}$$

where one assumes the ratios as a range-mean value plus a variation (Δ) from that value. Considering our measurements (Table II), the ranges of Φ_{epi}/Φ_{th} and $I_{\gamma_{(d+c)}}/\Phi_{th}$ are 4%–21% and 2×10^{-23} to 6×10^{-23} A·n^{-1}·cm^2·s, respectively. Therefore, Φ_{epi}/Φ_{th} is 12% and $I_{\gamma_{(d+c)}}/\Phi_{th}$ is 4×10^{-23} A·n^{-1}·cm^2·s. The maximum $\Delta(\Phi_{epi}/\Phi_{th})$ and $\Delta(I_{\gamma_{(d+c)}}/\Phi_{th})$ would be 9%—S_{epi} $\Delta(\Phi_{epi}/\Phi_{th}) < 10^{-22}$ A·n^{-1}·cm^2·s—and 2×10^{-23} A·n^{-1}·cm^2·s, which would have little impact on S_{mix}. According to the above mentioned values and considering S_{th} and S_{epi} as in Table II, it can be observed that

$$S_{mix} \sim S_{th} + S_{epi}\overline{\Phi_{epi}/\Phi_{th}} + \overline{I_{\gamma_{(d+c)}}\Big/\Phi_{th}} \tag{14}$$

TABLE III. Results of the Rh SPND based measurements during clinical trials: the expected theoretical (I_c) and measured currents (I_m), thermal neutron fluxes (Φ^c_{th} and Φ^m_{th}), calculated epithermal neutron flux (Φ^c_{epi}), and flux percentage differences ($\Delta^{\%}\Phi_{\text{th}}$) obtained for the reference points. MU column shows the average beam monitor units during the treatment.

Patient	MU (mV)	I_c (pA)	I_m (pA)	Φ^c_{th} (10^8 n·cm^{-2}·s^{-1})	Φ^c_{epi} (10^8 n·cm^{-2}·s^{-1})	Φ^c_{epi}/Φ^c_{th} (%)	Φ^m_{th} (10^8 n·cm^{-2}·s^{-1})	$\Delta^{\%}\Phi_{\text{th}}$ (%)
3—C1	300	0.94 ± 0.16	1.22 ± 0.01	5.00 ± 0.85	1.17 ± 0.15	23 ± 5	6.51 ± 0.19	30
3—C2	306	1.15 ± 0.20	1.40 ± 0.01	6.10 ± 1.04	1.49 ± 0.19	24 ± 5	7.45 ± 0.21	22
3—C3	306	0.058 ± 0.005	0.062 ± 0.020	0.31 ± 0.02	0.077 ± 0.003	25 ± 5	0.331 ± 0.014	7
4	306	0.76 ± 0.02	0.708 ± 0.012	3.90 ± 0.04	0.91 ± 0.01	23.3 ± 0.3	3.62 ± 0.12	−7
5	300	1.00 ± 0.03	0.746 ± 0.007	5.11 ± 0.05	1.23 ± 0.01	24.1 ± 0.3	3.82 ± 0.11	−25
6	300	1.16 ± 0.04	1.02 ± 0.01	6.19 ± 0.12	1.41 ± 0.03	22.8 ± 0.3	5.45 ± 0.16	−12

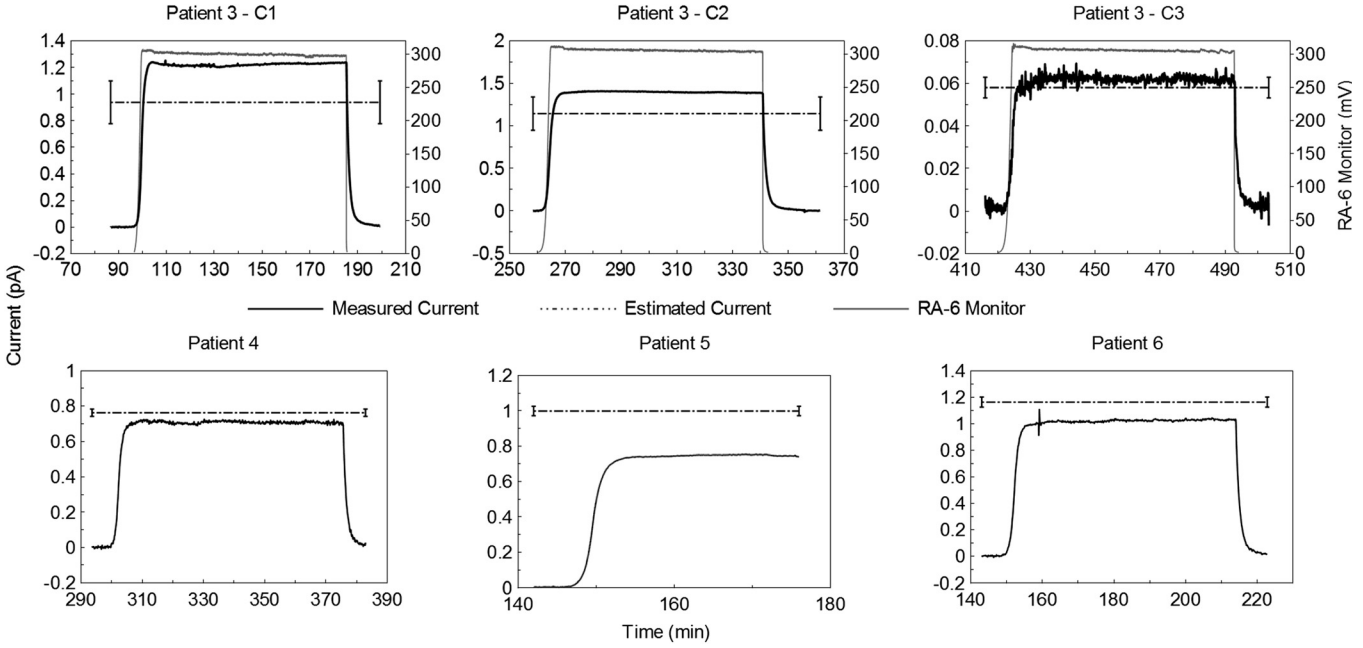

FIG. 4. Evolution of measured currents i_r and RA-6 beam monitor during irradiations. The currents I_c estimated from the planning are also presented.

is approximately 1.97×10^{-21} A·n^{-1}·cm^2·s, which is in agreement with the value of S_{mix} in that same table considering that the uncertainty is 5×10^{-23} A·n^{-1}·cm^2·s and includes the measurement uncertainties as well as the departures from the mean value introduced by the different flux compositions. From another point of view, the ratio between the maximum and minimum local S_{mix} is 1.03 ± 0.08 (with and without compensation for gamma dose variations), while the ratio between maximum and minimum epithermal-to-thermal flux is 5.3 ± 0.2. This shows the low impact of epithermal contributions under the range of evaluated conditions.

The uncertainties of the thermal neutron sensitivities are about 7% and are primarily due to the uncertainty of activity measurements for each activation wire used for the calibration. However, if the detector is used only for relative comparisons in a given spectrum, currents instead of fluxes can be directly compared. Since, under constant fluxes over 4×10^8 n·cm^{-2}·s^{-1}, current uncertainties are approximately 1% or less (Table III); the Rh SPND is capable of discriminating between thermal neutron flux values that differ by much less than 7% assuming that the overall spectrum is the same in both cases. This is an important advantage compared to activation methods.

The gamma response of the detector showed in Table I, $I_m^{\text{Zry}-4}$, is about 6%–8% of I_m and is therefore not negligible. This is a consequence of the considerable cable length exposed to the radiation fields. The thermal column is about 3 m in length and calibration positions were selected near the middle of the column. Thus, about 1.5 m cable length remained inside the column for each detector. However, this would not be the general situation in BNCT facilities with externally collimated beams, where the SPND detectors of interest can be installed in a manner where only a few centimeters of cable are irradiated and gamma induced currents are minimized.

Based on these results, it is concluded that the Rh SPND is well suited to assess thermal neutron fluxes in spectra having nearly Maxwell–Boltzmann shapes and epithermal-to-thermal ratios up to 21%. For cases where these conditions are not fulfilled, an appropriate *in situ* recalibration should be done.

IV.B. Rh SPND based flux measurements during clinical trials

The results of the use of the Rh SPND during clinical trials show differences between measured and calculated fluxes that range from −25% to +30%. These differences cannot be explained in terms of the uncertainty in the sensitivity or in the current readings. However, they could be explained in terms of differences between the planning and actual irradiation conditions, emphasizing the importance of on-line local flux measurement during treatment. Part of the difference can be attributed to the fact that the measurement points are superficial and, consequently, planning software cannot accurately render fluxes for minute volumes outside the irradiation model (patient's body). Estimated errors due to this effect are lower than 17% for patient 3—C1 and C2, 8% for patient 3—C3, 1% for patients 4 and 5, and 2% for patient 6 (uncertainty in Φ_{th}^c, Table III). Another source of differences is related to the positioning of the patient at the time of irradiation. During the treatment, every effort is made to place the patient as planned but slight movements of the patient can occur, leading to changes in flux. In summary, the Rh SPND based measurements allow determination of the actual thermal flux delivered to the reference points in order to detect and quantify any departure from planning conditions.

The calculated epithermal-to-thermal flux ratios for the treatments are larger (1.2 times at most) than the maximum ratio, 21%, considered during the calibration process.

However, given that local S_{mix} varies less than 11% with a variation of epithermal-to-thermal flux ratio from 4% to 21%, one would not expect a meaningful change in global S_{mix} when that ratio is 25%.

Additionally, the stability of the measurements throughout the irradiation sessions has been demonstrated in this work, as can be seen in Fig. 4. High stability in the measurements implies a similar level of stability in the fluxes impinging on the points where the detectors were positioned. In order to obtain an estimation of system stability, the neutron source behavior was first analyzed. The beam monitor signal with the reactor power in steady state showed a variability (standard deviation to mean value ratio) of less than 1% throughout the treatment. This is consistent with the expected level of stability of the SPND measuring system. From the typical current measurement errors shown in Table III, it is seen that the system variability is less than 3%. Additionally, as deviations due to temporal variations are included in those typical errors, such deviations are lower than the reported percentages. In general, current drifts from stable values during the irradiation were coincident with slight patient displacement from the original position (seen in the video monitor) or with reactor power-up and power-down (Fig. 4, top left). This shows that rapid changes can be detected in real time in spite of the longest half life of ^{104}Rh that produces a *setting time* (time to reach the 99% of the signal in steady state) of 14 min. In irradiations with many and fast changes, the dynamic compensation method could be used to detect sudden changes correctly in order to improve the online flux measurement.[10]

V. CONCLUSIONS

The particular design of SPND described in this work can be considered as having a pure thermal response in spectra with up to 12% of epithermal-to-thermal neutron flux ratio and a Maxwell–Boltzmann-like distribution in the thermal region and $1/E$ distribution in the epithermal region. In addition, this particular design of SPND can be used in beams similar to the original RA-6 mixed-spectrum BNCT beam as a neutron thermal indication, despite the known presence of gamma and epithermal neutron contributions, using a derived mixed thermal neutron sensitivity of $1.95 \pm 0.05 \times 10^{-21}$ $A{\cdot}n^{-1}{\cdot}cm^2{\cdot}s$ as described in this work.

The utilization of the detector during clinical trials showed the applicability of the system to detect local fluxes in real time during BNCT patient irradiations and the capability to provide measurements with sufficient accuracy to evaluate the quality of the treatment.

From the perspective of BNCT clinical trials, the self-powered detector could be used as a completely independent system to determine whether fluxes consistent with planned values have been delivered to patients. Moreover, since the SPND has the advantage of implantability, neutron fluxes just under the skin can be also monitored during treatments. This is of major importance in BNCT, particularly for cutaneous melanoma treatments in which normal skin is defined as a superficial layer of a few millimeters in depth and is considered the organ that limits the deliverable radiation dose.

ACKNOWLEDGMENTS

The authors greatly appreciate patients' collaboration. The authors also would like to thank the RA-3, RA-6, and specially RA-1 operation and radioprotection teams. Special thanks go to L. Pecos and L. Zarza from RA-3 and F. Sporleder from RA-6 for helping in the SPND characterization.

[a]Author to whom correspondence should be addressed. Electronic mail: miller@cae.cnea.gov.ar; Telephone: 54-11-6779-8327; Fax: 54-11-6779-8433.

[1]E. Browne, J. M. Dairiki, R. E. Doebler, A. A. Shihab-Eldin, L. J. Jardine, J. K. Tuli, and A. B. Buyrn, in *Table of Isotopes*, 7th ed., edited by C. Lederer (Wiley, New York, 1978).

[2]A. B. Rosenfeld, M. Yudelev, M. L. F. Lerch, I. Cornelius, P. Griffin, V. L. Perevertailo, I. E. Anokhin, O. S. Zinets, V. I. Khivrich, M. Pinkovskaya, D. Alexiev, and M. Reinhard, "Neutron dosimetry with planar silicon p-i-n diodes," IEEE Trans. Nucl. Sci. **NS-50**, 2367–2372 (2003).

[3]G. I. Kaplan *et al.*, "Semiconductor detectors for in-phantom thermal neutron flux and boron dose measurements in BNCT and fast neutron therapy," in *Frontiers in Neutron Capture Therapy*, edited by M. F. Hawthorne, K. Shelly, and R. J. Wiersema (Kluwer Academic/Plenum, New York, 2001), pp. 1175–1180.

[4]A. B. Rosenfeld, G. Kaplan, M. Carolan, B. Allen, O. Zinets, V. Khivrich, and P. G. Litovchenko, "Application of P-I-N diodes and MOSFET for dosimeter in gamma and neutron fields," Radiat. Prot. Dosim. **84**, 349–352 (1999).

[5]A. B. Rosenfeld, "Semiconductor dosimetry in BNCT: Present and future," in Review Proceedings of 8th International Symposium on Neutron Capture Therapy for Cancer, La Jolla, CA, 14–18 September, 1998.

[6]M. G. Carolan, A. B. Rosenfeld, S. Wallace, H. Mariaty, G. J. Storr, V. I. K. Khivrich, B. J. Allen, and J. N. Mathur, "Silicon dosimetric diode for BNCT using epithermal neutron sources," in *Proceedings of the First International Workshop on Accelerator-Based Neutron Sources for Boron Neutron Capture Therapy*, edited by D. W. Nigg and R. J. Wiersema, US DoE Conference Report No. CONF-940976 (US DoE, Washington DC, 1995), pp. 299–309.

[7]M. Ishikawa, N. Unesaki, T. Kobayashi, Y. Sakurai, K. Tanaka, S. Endo, and M. Hoshi, "Real-time estimation of neutron flux during BNCT treatment using plastic scintillation detector with optical fiber," in *Proceedings of the Tenth International Congress on Neutron Capture Therapy*, edited by W. Sauerwein, R. Moss, and A. Wittig, (Monduzzi Editore, Bologna, 2002), pp. 443–447.

[8]M. Ishikawa, K. Ono, Y. Sakurai, H. Unesaki, A. Uritani, G. Bengua, T. Kobayashi, K. Tanaka, and T. Kosaco, "Development of real-time thermal neutron monitor using boron-loaded plastic scintillator with optical fiber for boron neutron capture therapy," Appl. Radiat. Isot. **61**, 775–779 (2004).

[9]M. E. Miller, L. E. Mariani, M. L. Sztejnberg Gonçalves-Carralves, M. Skumanic, and S. I. Thorp, "Implantable self-powered detector for online determination of neutron flux in patients during NCT treatment," Appl. Radiat. Isot. **61**, 1033–1037 (2004).

[10]L. E. Mariani, M. Skumanic, and M. L. Sztejnberg Gonçalves-Carralves, "Proyecto Final de Ingeniería: Detector autoenergizado, implantable en pacientes sometidos a NCT, para medición de flujo neutrónico en tiempo real," in *UAIyC-Comisión Nacional de Energía Atómica and FICEN-Universidad Favaloro* (Universidad Favaloro, Buenos Aires, 2004).

[11]Pointwise ENDF-VI Library, in *Table of Nuclides* (Nuclear Data Evaluation Laboratory, Korea Atomic Energy Research Institute, Daejeon, Korea, 2000).

[12]J. F. Briesmeister, *MCNP—A General Monte Carlo N-Particle Transport Code 12625-M* (University of California, Los Alamos, 1997).

[13]H. R. Blaumann, S. J. González, J. Longhino, G. A. Santa Cruz, O. A. Calzetta Larrieu, M. R. Bonomi, and B. M. C. Roth, "Boron neutron capture therapy of skin melanomas at the RA-6 reactor: A procedural approach to beam set up and performance evaluation for upcoming clinical trials," Med. Phys. **31**, 70–80 (2004).

[14]P. R. Menéndez, B. M. C. Roth, M. D. Pereira, M. R. Casal, S. J. González, D. B. Feld, G. A. Santa Cruz, J. Kessler, J. Longhino, H. Blaumann, R. Jiménez Rebagliati, O. A. Calzetta Larrieu, C. Fernández, S. I. Nievas, and S. J. Liberman, "BNCT for skin melanoma in extremities: Updated argentine clinical results," Appl. Radiat. Isot. **67**, S50–S53 (2009).

[15]S. J. González, M. R. Casal, G. A. Santa Cruz, M. R. Bonomi, R. Jiménez Rebagliati, D. G. Carando, H. R. Blaumann, M. A. Dagrosa, J. Longhino, O. A. Calceta Larrieu, D. B. Feld, S. Castiglia, B. M. C. Roth, P. Menéndez, D. Batistoni, and S. J. Liberman, "Detailed dosimetry and clinical outcome análisis for the argentine BNCT trials of cutaneous nodular melanoma," in *Advances in Neutron Capture Therapy 2006 Proceedings of ICNCT-12,* edited by Y. Nakagawa, T. Kobayashi, and H. Fukuda (International Society for Neutron Capture Therapy, Kagawa, Japan, 2006), pp. 485–488.
[16]G. F. Knoll, *Radiation Detection and Measurement* (Wiley, New York, 1989).
[17]M. Miller, J. Quintana, J. Ojeda, S. Langan, S. Thorp, E. Pozzi, M. Sztejnberg, G. Estryk, R. Nosal, E. Saire, H. Agrazar, and F. Graiño, "New irradiation facility for biomedical applications at RA-3 reactor thermal column," Appl. Radiat. Isot. **67**, S226–S229 (2009).
[18]E. Pozzi, D. W. Nigg, M. Miller, S. I. Thorp, A. E. Schwint, E. M. Heber, V. A. Trivilin, L. Zarza, and G. Estryk, "A small-animal irradiation facility for neutron capture therapy research at the RA-3 research reactor," *Proceedings of the 2007 ANS Winter Meeting. Research Reactor*, Trans. Am. Nucl. Soc. **97**, 309–311 (2007).
[19]IAEA, "Neutron fluence measurements," IAEA Technical Report Series No. 107 (IAEA, Vienna, 1970).
[20]S. J. González, G. A. Santa Cruz, W. S. Kiger III, J. T. Goorley, M. R. Palmer, P. M. Busse, and R. G. Zamenhof, "NCTPlan, the new PC version of MacNCTPlan: Improvements and verification of a BNCT treatment planning system," in *Proceedings of the Tenth International Congress on Neutron Capture Therapy*, edited by W. Sauerwein, R. Moss, and A. Wittig (Monduzzi Editore, Bologna, 2002), pp. 557–561.
[21]W. S. Kiger III, G. A. Santa Cruz, S. J. González, F. Y. Hsu, K. J. Riley, P. J. Binns, O. K. Harling, M. R. Palmer, P. M. Busse, and R. G. Zamenhof, "Verification and validation of the NCTPlan treatment planning program," in *Proceedings of the Tenth International Congress on Neutron Capture Therapy*, edited by W. Sauerwein, R. Moss, and A. Wittig (Monduzzi Editore, Bologna, 2002), pp. 613–616.
[22]S. J. González, Monitoreo Paciente No. 4 12/04/05, Technical Report CNEA (CNEA, 2005).
[23]S. Gossio, D. G. Carando, and S. J. González, "A computational dosimetry tool for the study of tumor doses and skin toxicities in BNCT," Appl. Radiat. Isot. **67**, S145–S148 (2009).